Application of the Self-Assembled Monolayer (SAM) Model to Dithiophosphate and Dithiocarbamate Engine Wear Inhibitors

Yanhua Zhou,[†] Shaoyi Jiang,[†,||] Tahir Çağın,[†] Elaine S. Yamaguchi,[‡] Rawls Frazier,[‡] Andrew Ho,[‡] Yongchun Tang,[‡] and William A. Goddard, III*,[†]

Materials and Process Simulation Center, Beckman Institute (139-74), Division of Chemistry and Chemical Engineering, California Institute of Technology, Pasadena, California 91125, Chevron Corporation, 100 Chevron Way, Richmond, California 94802

Received: March 8, 1999; In Final Form: December 23, 1999

In previous studies of dithiophosphate [DTP = $S_2P(OR)_2$] wear inhibitors bound to an oxidized iron surface, we found that the cohesive energy of the self-assembled monolayers (SAM) for DTP molecules with various organic R groups correlates with the wear inhibition observed in full engine experiments. In this paper we expand these calculations to consider dynamics at 500 K and then use the SAM model to predict new candidates for wear inhibitors. Using molecular dynamics (MD) simulations at 500 K, we show that the SAM has one DTP per two surface Fe sites of iron oxide. At this coverage we find that the cohesive energy of the SAM at 500 K is in the sequence 2-alkyl > 1-alkyl > aryl (e.g., *i*Pr > *i*Bu > Ph) which again correlates with wear inhibitor performance observed in engine tests. We then considered 7 novel DTPs and predict that R = cyclo-hexyl, *n*Pr, and benzyl may perform as well as *i*Pr. We then used the SAM wear inhibitor model to assess the likely performance of 11 novel classes of potential wear inhibitors. On the basis of this model we selected dithiocarbamates (DTC) as the best candidate to supplement DTP. We then considered a number of possible alkyl substitutions for DTC. The SAM model suggests that iC_5 and nC_3 are the best candidates, followed closely by iC_3.

I. Introduction

Zinc dithiophosphates [$Zn(DTP)_2$] (DTP, **1**) have been used

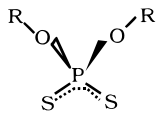

R=organic

1 DTP

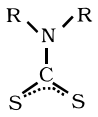

R=organic

2 DTC

for several decades[1] as the most effective and economic lubricant antiwear additive. Although $Zn(DTP)_2$ reduces wear to acceptable levels in modern engines, the DTP contains phosphorus. Since recent industrial specifications have imposed limitations on the maximum phosphorus content that can be used in lubricant additives, it is important to find a substitute for DTP. Such restrictions on the maximum allowable phosphorus contents in engine lubricant formulations could lead to considerable difficulty in maintaining satisfactory wear protection in engines.[2]

The search for a DTP replacement without phosphorus which can provide wear protection to engine surfaces as effective as $Zn(DTP)_2$ presents a strong challenge to the oil industry. There are a large number[3] of potential lubricant additives that might possibly help control friction, deposits, corrosion, oxidation, and rust. This makes an empirical search laborious and expensive. A serious impediment to this search is that the factors underlying good wear performance are not well understood. Furthermore, a complete engine test for a new wear inhibitor might cost $150000, making it too expensive for random combinatorial experimentals. Consequently, we explored the use of atomistic molecular dynamics (MD) simulations to provide guidance in prioritizing new materials for experimental engine tests.[2,4] This led to the self-assembled monolayer (SAM) model[4] in which the calculated cohesive energy for the SAM was found to correlate with actual engine performance of the wear inhibitor.

In this paper we extended the SAM model to use the cohesive energy calculated from MD at 500 K. Since the temperature of camshaft surface in sequence V-D and III-C engine tests ranges from 150 to 220 °C,[10b] we choose the maximum temperature for our dynamics runs. We find that the SAM model still correlates with actual engine tests. We also considered the differential adsorption of various concentrations of the DTP on the surface to determine the coverage at 500 K. We find that the optimum is 1 DTP per each two surface Fe sites (as predicted in our earlier minimization studies[4]). We then considered some novel DTPs, where we find three candidates that might improve performance.

Next we considered a number of candidate wear inhibitors not containing phosphorus and used the SAM model to predict relative performance. Based on these calculations we selected dithiocarbamates (DTC, **2**) as the best candidate. Considering various alkyl ligands on the DTC, we used the SAM model to predict the relative performance.

* To whom correspondence should be addressed.
[†] Materials and Process Simulation Center.
[||] Currently at Kansas State University, Department of Chemical Engineering.
[‡] Chevron Corporation.

10.1021/jp9908146 CCC: $19.00
Published on Web 03/16/2000

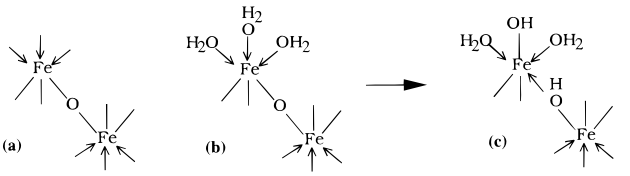

Figure 1. A double layer of α-Fe_2O_3. (a) Bulk α-Fe_2O_3. Fe is in a distorted octahedral site with three CPI bonds to O atoms (lines) and three DA bonds to O atoms (arrows). (b) Unreconstructed (0001) surface of α-Fe_2O_3 with three H_2O per surface Fe. The surface Fe has three CPI bonds to subsurface O atoms (lines) and three DA bonds to the surface H_2O (arrows). (c) Reconstructed (0001) surface of α-Fe_2O_3. A hydrogen from the surface H_2O is transformed to the subsurface O atom, leading to two H_2O and two OH per reconstruction site. Each Fe still has three CPI bonds and three DA bonds.

Section II describes in detail the computer models for iron-oxide surface and the construction of SAM films. Section III reports several properties from the simulation results for the DTP at various coverages, leading to the conclusion that the optimum SAM has $^1/_2$ coverage. Section IV correlates these results on DTP with the observed wear performance, showing that the SAM model correlates well. The model is used to assess seven new candidates. In section V we consider 11 new classes of non-phosphorus wear inhibitors, concluding that DTC is best. The best organic groups of DTC are then selected based on the SAM model. The conclusions are summarized in section VI.

II. Calculations

II.A. The Computational Model. There is only a rudimentary understanding of the mechanism by which $Zn(DTP)_2$ prevents wear. It is generally believed that they can adsorb on the metal surfaces to form a thin film, which prevents direct metal-metal contact, thereby reducing wear. A simplified scenario is that $Zn(DTP)_2$ initially physisorbed on the surface (mainly van der Waals interactions) decomposes and reacts with the surface to form a chemisorbed zinc-depleted layer. This is supported by experiments on adsorption of $Zn(DTP)_2$ on steel surfaces.[5] However, little is known about the details of how $Zn(DTP)_2$ react with the surface, and there are a number of ways in which $Zn(DTP)_2$ can decompose,[6] leading to a wide variety of chemisorption products including iron sulfide, phosphates, and thiophosphates that might form on the surface.

In this study, we assume that Zn has been dissociated from the DTP in contact with the metal surface, but we assume that the DTP group is not further decomposed upon adsorption.[7] Thus, a SAM of DTP is formed on the surface. Using a force field (FF)[8] based on quantum mechanics (QM), we calculated the adsorption of DTP on the surface and the stability of the DTP overlayer as a function of concentration.

The effectiveness of $Zn(DTP)_2$ in protecting metal surfaces is expected to depend on the concentration of additives attached to the surfaces. This is affected by many factors, including additive concentration, time, temperature, and the nature of surfaces. A number of experiments have been carried out to investigate the kinetic aspects of the adsorption process.[5,9] It was found that the equilibrium amount adsorbed on the γ-Fe_2O_3 surface saturates at a value of 55 Å^2/molecule that is independent of time and concentration. Our modeling calculations (on α-Fe_2O_3) also indicate a clearly defined saturation coverage of one adsorbate molecule per two surface iron atoms for all the DTP and DTC monolayers investigated. Above this coverage adsorbate−adsorbate interactions make adsorption on the surface significantly less favorable. This SAM leads to an area per adsorbed molecule of 44 Å^2 (α-Fe_2O_3), about 20% lower than the experimental value for γ-Fe_2O_3.

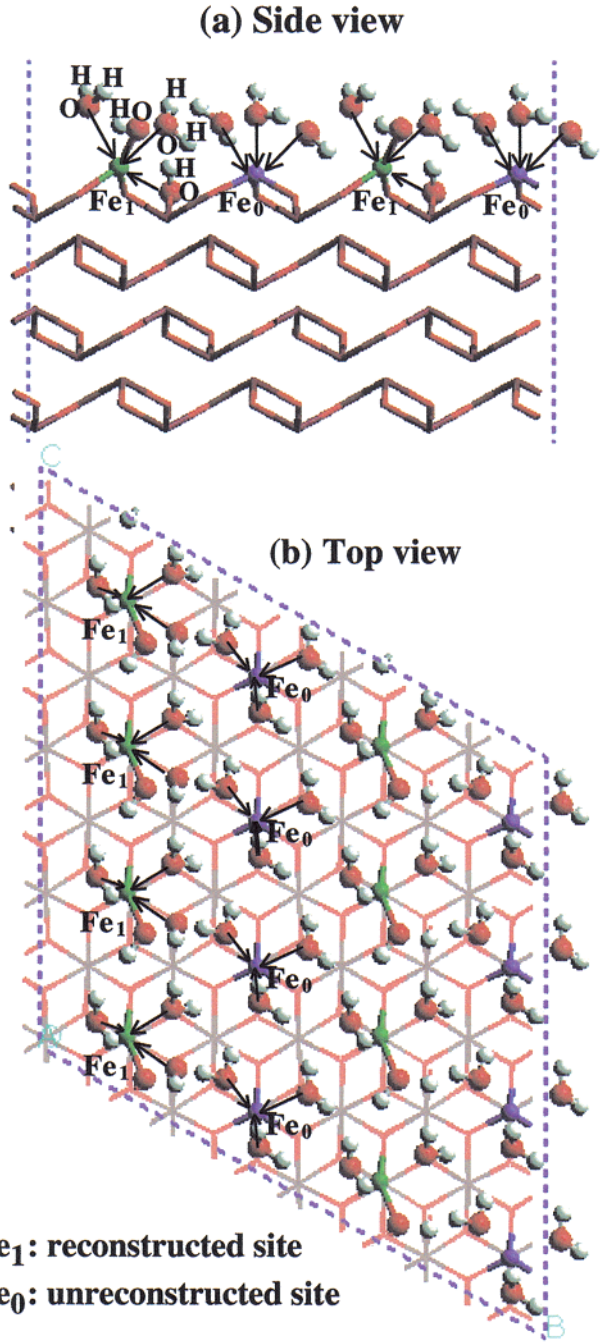

Figure 2. The reconstructed α-Fe_2O_3 (0001)−(4 × 4) surface. The surface Fe sites are highlighted by the balls (blue for unconstructed; green for reconstructed). The CPI bonds are denoted by blue and green cylinders, and DA bonds by arrows. (a) Side view showing only the atoms in 4 × 4 unit cell. (b) Top view of the 4 × 4 cell.

The antiwear effectiveness of $Zn(DTP)_2$ is observed to depend dramatically on the nature of the R groups,[10] which controls the rate of thermal decomposition and subsequent reactivity. Commercial $Zn(DTP)_2$ usually contain a blend of species with three types of R groups: 1. secondary alkyl [we use isopropyl (*i*Pr) as the prototype], 2. primary alkyl [we use isobutyl (*i*Bu) as the prototype], and 3. aryl [we use phenyl (Ph) as the prototype].

Various engine tests[10] simulating a wide-range of engine operating conditions have consistently shown that the secondary alkyl $Zn(DTP)_2$ provides the lowest wear rate and the best

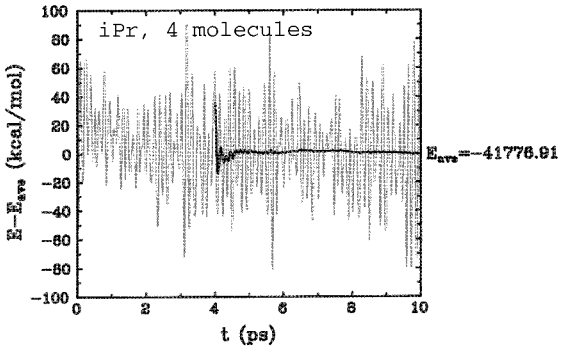

Figure 3. Deviation from the average energy of the SAM structure as a function of time in a 10 ps MD run for the case of 4 *i*Pr-DTP molecules on the surface. The thick line is the running average starting from 4 ps.

antiwear performance, followed by the primary alkyl $Zn(DTP)_2$ and aryl $Zn(DTP)_2$:

$$\text{wear: } i\text{Pr} < i\text{Bu} < \text{Ph}$$

Many attempts have been made to correlate the differences in performance with *ex situ* experiments (friction, wear, spectroscopy). Although no simple explanations account for all the observed variations, it seems that higher antiwear effectiveness is associated with lower thermal stability of $Zn(DTP)_2$,[11] stronger bonding between the P−S groups to the surfaces,[7] and larger amounts of additive adsorption.[5,9] Our previous studies[4] suggested that an important factor controlling the performance is the cohesive energies of the SAM formed by a DTP monolayers (at 1/2 coverage).

II.B. Force Fields. To perform dynamics simulations of such systems, it is essential to have an accurate description of the forces. For the studies with DTP we previously[2,4,13,14] combined QM on Fe clusters containing DTP with the Dreiding force field (FF)[15] to obtain a new DTP/Fe_2O_3 FF. This uses charge equilibration (QEq)[16] to predict the charges. This DTP/Fe_2O_3 FF uses Morse nonbond terms to describe the Fe···S interactions so that dissociation and rebinding is allowed. For DTC/Fe_2O_3 we use the parameters from the DTP/Fe_2O_3 FF if defined and otherwise take them from the Dreiding FF.

II.C. Surface. The wear surfaces in an engine involve a steel alloy that is probably partially oxidized. To represent this system we consider the cleavage surface (0001) of α-Fe_2O_3 as a model for the oxidized surfaces. The iron atom in α-Fe_2O_3 crystal is in a distorted octahedral site with three bonds at 1.946 Å and three at 2.116 Å.[17]

In the generalized valence bond (GVB) model of this surface,[2,4,13,14] we consider that the three short Fe−O bonds are covalent, partially ionic (CPI) bonds and the three long Fe−O bonds are of donor−acceptor (DA) nature. A schematic representation is in Figure 1a where lines indicate CPI bonds

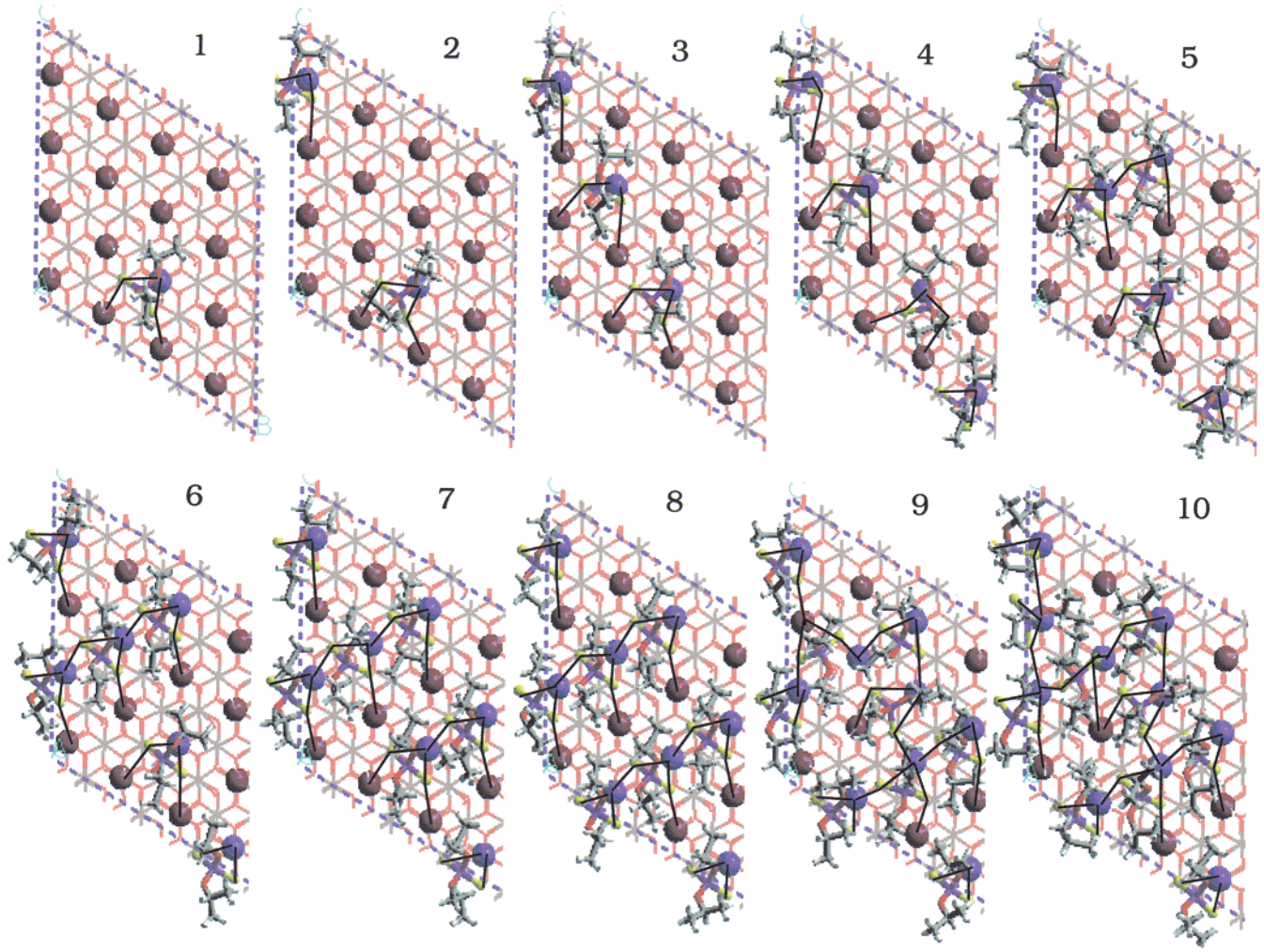

Figure 4. Top view of the SAM structure for 1 to 10 *i*Pr-DTP molecules on the α-Fe_2O_3 (001)−(4 × 4) surface. The surface Fe sites are shown as balls. Red balls denote the original reconstructed Fe site, and blue balls are the Fe site with OH removed and replaced by a DTP molecule (cylinders). Lines indicate the bridge position of S bound to Fe atoms.

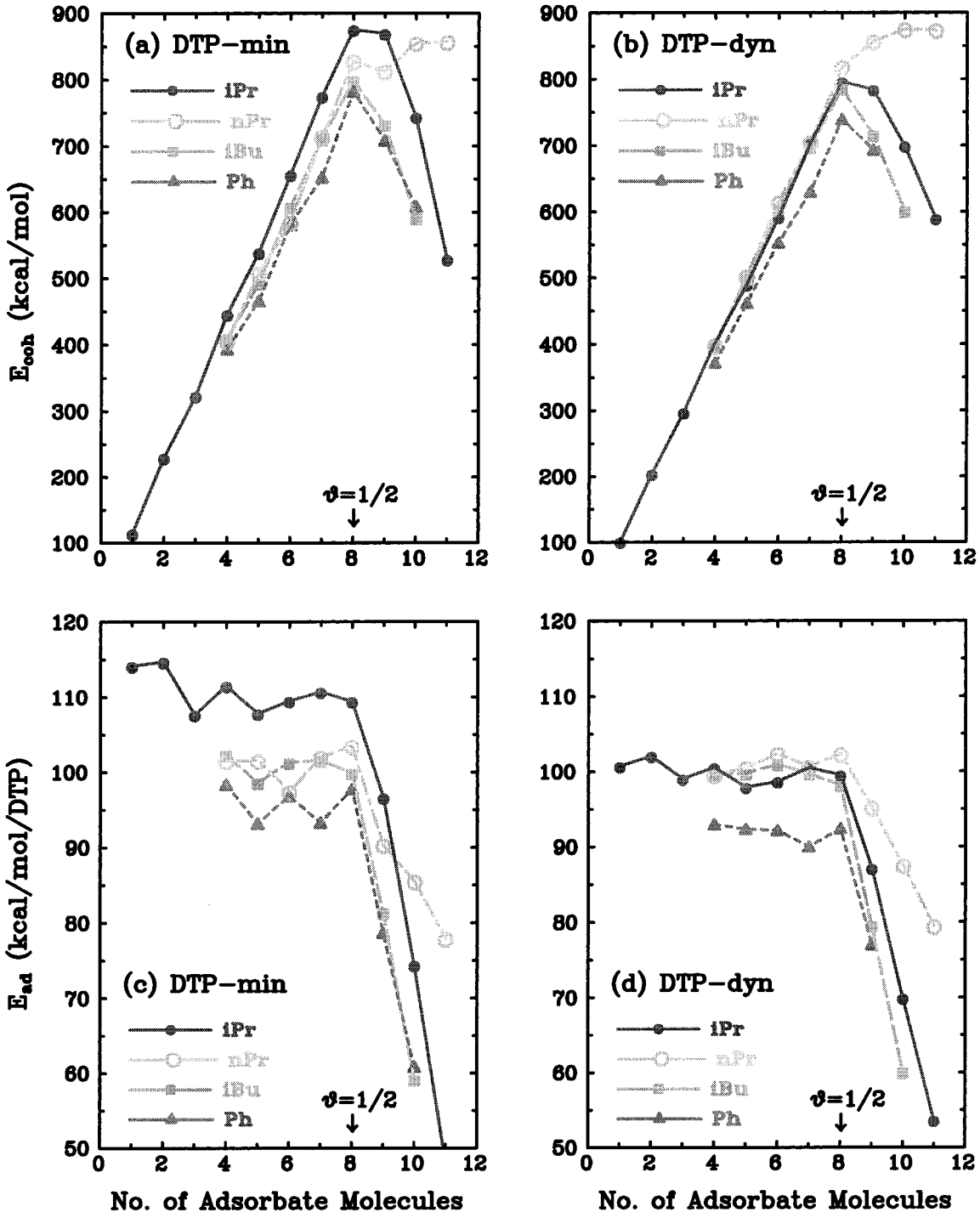

Figure 5. Cohesive enregy and adsorption energy as a function of surface coverage for DTP molecules: (a) E_{coh} from minimized structures, (b) E_{coh} from 10 ps of MD simulations at 500 K (for a coverage of 8 adsorbate molecules we did 20 ps), (c) E_{ad} from minimized structures, and (d) E_{ad} from 10 ps of MD simulations at 500 K.

and arrows DA bonds. In the GVB model there are no CPI bond across the (0001) plane, suggesting that the (0001) surface has the lowest energy, as observed.[18] This model suggests that exposed to air or water, the bonds would be recoordinated to H_2O or OH^- as in Figure 1b, where the top Fe is at the surface. However, this surface can reconstruct as indicated in Figure 1c. Here we start with each surface Fe site initially coordinated to three H_2O. In the reconstruction, one solvent H_2O molecule is replaced by an OH forming a covalent−ionic bond to the surface Fe. This breaks a covalent−ionic bond from this surface Fe to a surface O. We then use the H of the original surface H_2O to bond this surface O to form an OH. The reconstructed surface preserves the octahedral coordination of all Fe. It leads to an OH:H_2O ratio of 1:1 (the equilibrium ratio of OH to H_2O on the surface depends on the pH and solvent).

All calculations presented below are based on a 4 × 4 supercell of this reconstructed α-Fe_2O_3 (0001) surface (Figure 2). This 4 × 4 unit cell is rhombohedral with a long diagonal of 34.90 Å and a short diagonal of 20.15 Å. Each surface contains 16 Fe binding sites with a spacing between neighboring surface Fe atoms of 5.04 Å. As discussed above, each of the 16 surface Fe has one OH bound as does each of the 16 second-layer Fe. We used a slab thickness of four α-Fe_2O_3 layers (9 Å) on top of which was one layer of DTP. Adjacent slabs are

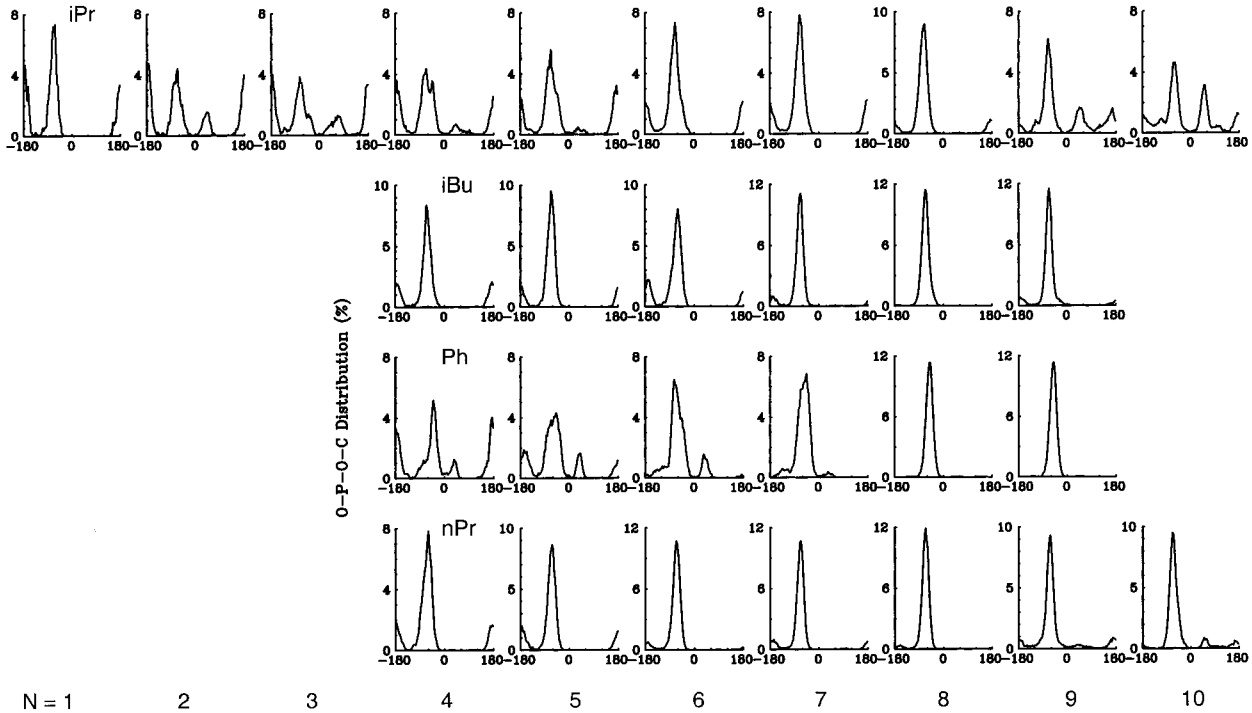

Figure 6. The discretized O−P−O−C torsional angle distribution (trans, gauche$^+$, gauche$^-$) as a function of coverage for DTP molecules, averaged over the 10 ps dynamics.

separated by a vacuum of 30 Å to 35 Å (allowing use of available programs written for 3-dimensional periodic boundary conditions[19]). In the calculations the real part of the Ewald sums was carried out over a single slab, but the Fourier reciprocal space terms include interactions between slabs. The larger the separation, the less interaction between the slabs and the more accurate results. However, too large a separations between the slabs leads to slow convergence of the Fourier reciprocal space terms. In our previous study,[4] we considered various separations between the slabs and found that a slab separation of 15−45 Å is appropriate in regard to the tradeoff between the accuracy and computing efficiency.

II.D. Self-Assembled Monolayer. We assume that the adsorbed $Zn(DTP)_2$ decomposes (for temperatures greater than 60 °C), leading to DTP bonded to surface Fe with loss of zinc from the surface. Since DTP can make one CPI bond and one DA bond,[3,4,13,14] we assume that it displaces one hydroxyl and one H_2O from the α-Fe_2O_3 (0001) leading to surface Fe atoms coordinated to four oxygens and one or two sulfurs. The electrostatic interactions between DTP and the surface Fe provide a large driving force for chemisorption and formation of a SAM. Our earlier calculations[4] indicate that this pathway is exothermic.

The sulfur atoms of the DTP bound to surface Fe atoms so that the molecules stand normal to the iron-oxide surface. We find that the most stable binding pattern for a layer of DTP to the surface is for the S atoms to bond to Fe atoms in bridge positions,[4] that is each S coordinates simultaneously to two nearest neighbor Fe atoms (see Figures 4 and 17).

II.E. Other Details. The long-range interactions are evaluated using Ewald summation with an accuracy parameter of 0.001 kcal/mol.[20] The NVT MD used a Hoover thermostat[21] with a time constant of 0.1 ps. The temperature is set at 500K for all the runs. The MD time step was 1 fs. Unless stated otherwise, the simulations were carried out for a period of 10 ps, which was sufficient for equilibration. Figure 3 shows the convergence of the total energy in a 10 ps MD run when four *i*Pr molecules are adsorbed on the surface, which is typical for the MD runs of all other cases. We see that the total energy convergences after the first 4 ps of equilibration. The running average after 4 ps (indicated by the thick line in Figure 3) is constant with fluctuations of less than 0.1%.

III. Results on DTP

Figure 4 shows the minimized structure of the SAM layers containing 1 to 10 *i*Pr adsorbate molecules on the surface. To construct the structures corresponding to various surface coverages, we started by replacing one OH with a DTP molecule, and progressively replaced additional OH's with DTPs. We carried out this procedure successively until either the adsorption energy drops significantly or all 16 surface Fe sites are covered by the DTPs.

For the first replacement, we removed an OH near the center of the unit cell and placed a DTP molecule nearby. We then minimized the structure. Starting with this optimal structure, we added a second molecule to the surface, by placing the OH far from the existing molecules on the surface. Again the structure was minimized. At low coverages ($<^1/_4$), there is sufficient space on the surface so that the adsorption energy is independent of exactly where the molecules are placed, as long as they are far from each other. As more molecules are added to the surface, it becomes important how to place the molecule DTP to minimize molecule−molecule interactions. We tested several possible adsorption configurations at each coverage. The resulting optimal configuration at various coverages are shown in Figure 4. The surface Fe site covered by a DTP molecule is indicated by the blue ball, as compared to the uncovered Fe site (red ball). The systematic trend of our adsorption energies suggest that the packing patterns shown in Figure 4 are close to the optimal packing at each coverage.

From the minimized structure at each coverage, we carried out MD simulations at 500 K for 10 ps (except for the *i*Pr, *i*Br, and Ph cases with eight molecules, which were run for 20 ps).

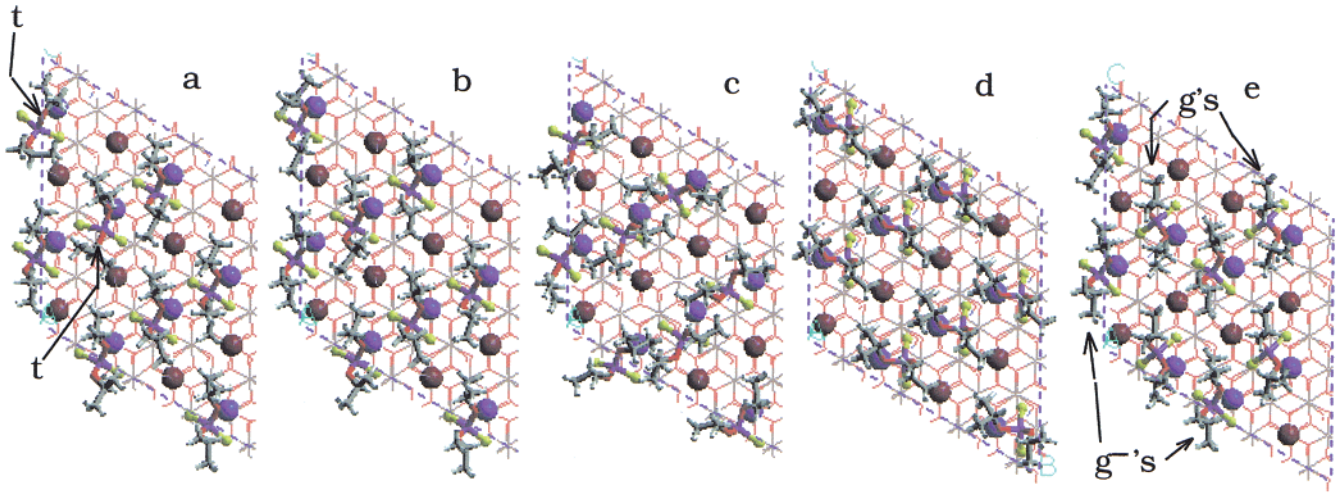

Figure 7. Top view of several SAM structures of *i*Pr-DTP at 1/2 coverage. (a) At the end of MD. Of the 16 torsional angles, 14 are g^- conformers and 2 are *t* conformers. This leads to a total energy of −43388 kcal/mol. (b) The two *t* conformers were manually converted to g^- conformers and reminimized (the energy drops 5 kcal/mol to −43393 kcal/mol). (c) All 16 conformers were changed to g^+, with the same S−Fe binding direction. Here the molecules are overpacked along the direction of the short diagonal of the parallelogram. This leads to an energy of −43273 kcal/mol, 120 kcal/mol worse than that in (b). (d) Same as (c), except the S−Fe binding direction is rotated 60°. This leads to an energy of −43413 kcal/mol, 20 kcal/mol better than that in (b). (e) A packing pattern with 50% g^- and 50% *g* conformers alternating on the Fe binding sites. This leads to an energy of −43395 kcal/mol, 2 kcal/mol better than that in (b). Essentially, (a), (b), (d), and (e) are all equivalent.

We then selected from the MD trajectory the structure with the lowest potential energy and reminimized. The results shown below under the "minimization" are based on these reminimized structures.

III.A. Adsorption Energy. The cohesive energy for *N* molecules adsorbed on the surface is calculated as

$$E_{coh} = -(E_{surf+SAM} - E_{surf} - NE_{mol}) \quad (1)$$

$$E_{ad} = E_{coh}/N$$

where $E_{surf+SAM}$ is the total energy of the Fe_2O_3 surface plus SAM, E_{surf} is the total energy of the Fe_2O_3 surface only, and E_{mol} is the total energy of the isolated SAM molecule in the gas phase. The molar adsorption energy E_{ad} is then obtained by normalizing with the number of adsorbate molecules.

In calculating the energy of the free surface, we assume that the surface Fe's have been reconstructed and that two H_2O on the free surface have been removed from the Fe site. The energy cost of doing this has not been included in (1). Consequently, the calculated adsorption energies are quite high.[22] However, the corrections will be the same for all DTP and DTC systems and hence will not effect the relative adsorption energy. The total energy of the surface is −41948.3 kcal/mol from minimization and −41332.8 kcal/mol at 500 K averaged from a 30 ps MD run.

The cohesive energy and adsorption energy results for DTP are summarized in Figure 5a,c (from minimization) and 5b,d [from MD simulations (500 K)]. The cohesive energy peaks at $\theta = {}^8/_{16} = {}^1/_2$, except for *n*Pr. Similarly, the adsorption energy is essentially independent of number of adsorbate molecules up to a coverage of $\theta = {}^1/_2$ and then drops precipitously for high coverage. The considerable reduction in cohesive energy and adsorption energy indicates that ligand−ligand interactions between neighboring adsorbed molecules become significant for surface coverages higher than ${}^1/_2$.

In contrast to all other cases, the cohesive energy of nPr has a maximum at $\theta = {}^5/_8$. This higher peak coverage indicates that the same surface can accommodate slightly more *n*Pr than *i*Pr molecules. This may arise because linear *n*Pr is thinner than

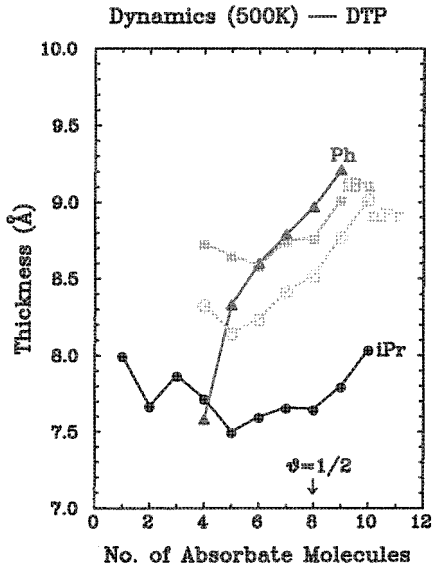

Figure 8. Monolayer thickness as a function of coverage for DTP molecules calculated from 10 ps MD at 500 K.

branched *i*Pr. Also it could be that *n*Pr, being more flexible than *i*Pr, can readjust to accommodate the insertion of more molecules on the surface without too many bad ligand−ligand contacts.

These results show that the phenyl case leads to cohesive energies systematically lower than the alkyl systems. At coverages higher than $\theta = {}^1/_2$, the MD results suggest that the size of the R group dominates, with higher binding energy in the sequence of *n*Pr ≈ *i*Pr ≈ *i*Bu > Ph. The minimization calculations also show the drop in adsorption energy above $\theta = {}^1/_2$ but lead to binding energies in the sequence *i*Pr > *n*Pr > *i*Bu > Ph. Using the standard deviations in the potential energy (typically 40 kcal/mol for the SAM structures and 0.4−0.8 kcal/mol for the isolated molecules) to estimate the uncertainty in binding energy suggests that the uncertainty in the adsorption energy calculated from (1) is approximately (i) 3 kcal/mol at $= {}^1/_4$, (ii) 2 kcal/mol at $= {}^1/_2$, and (iii) 1 kcal/mol at $= {}^3/_4$.

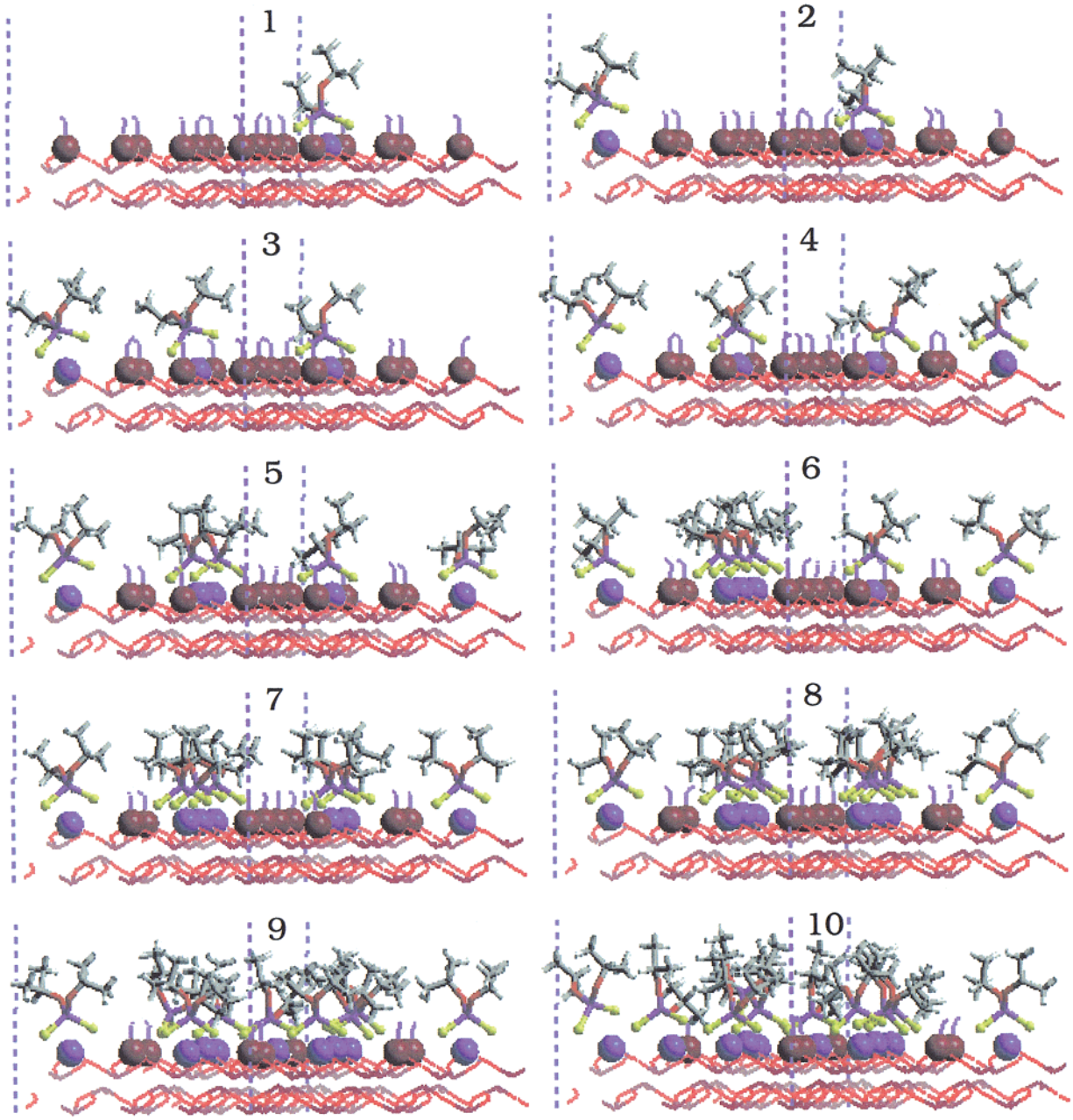

Figure 9. Side view of the SAM structure for 1 to 10 *i*Pr-DTP molecules on the surface (symbols same as in Figure 4).

Thus, the uncertainty in E_{ad} decreases as the number of adsorbate molecules increases.

III.B. Conformation Analysis. To understand how the conformations of the organic group of the SAM molecule affect binding, we analyzed the O−P−O−C torsional angle for each DTP molecule. The three most important conformers are *t* (180°), g^+ (66°), and g^- (−66°) conformers. Their definitions can be found in Figure 2 of ref 2. Figure 6 shows the percentage distribution of the torsional angles averaged over the dynamics at different surface coverages. We see that at $\theta = 1/2$ packing g^- conformer is the dominant conformer for all four DTP molecules, while the fractions of *t* and g^+ conformers increase at coverages below and above the half coverage.

For *i*Bu, Ph, and *n*Pr, the MD leads to the optimum packing ($\theta = 1/2$) that has the g^- conformation for all 16 torsional angles. However, *i*Pr has an optimum with 14 g^- and 2 *t* conformers (Figure 7a). Our process of building up the SAM by adding a new molecule to the structure at lower concentration allowed the entire structure (including the surface and molecules) to relax "naturally" in the minimization and dynamics processes. Thus, we did not alter the molecular conformation manually to make the packing more ordered. The two remaining *t* conformer in the case of *i*Pr suggested that this structure might not be fully relaxed. To test this, we manually transformed the two *t* conformers to g^-, leading to Figure 7b (all g^- conformers) with a total energy that is 5 kcal/mol lower than that of the built-up structure (Figure 7a). This leads to a cohesive energy larger by only 0.6 kcal/mol, which is within the estimated error of E_{ad}. Starting with the all g^- conformers we carried out 20 ps of MD at 500 K, and found that all conformers remain g^-, suggesting that this is the most stable conformation in the SAM.

To understand why the g^- conformation is best, we converted all conformations to g^+, leading to Figure 7c. Obviously, Figure 7c has the molecules overpacked in the direction of the short

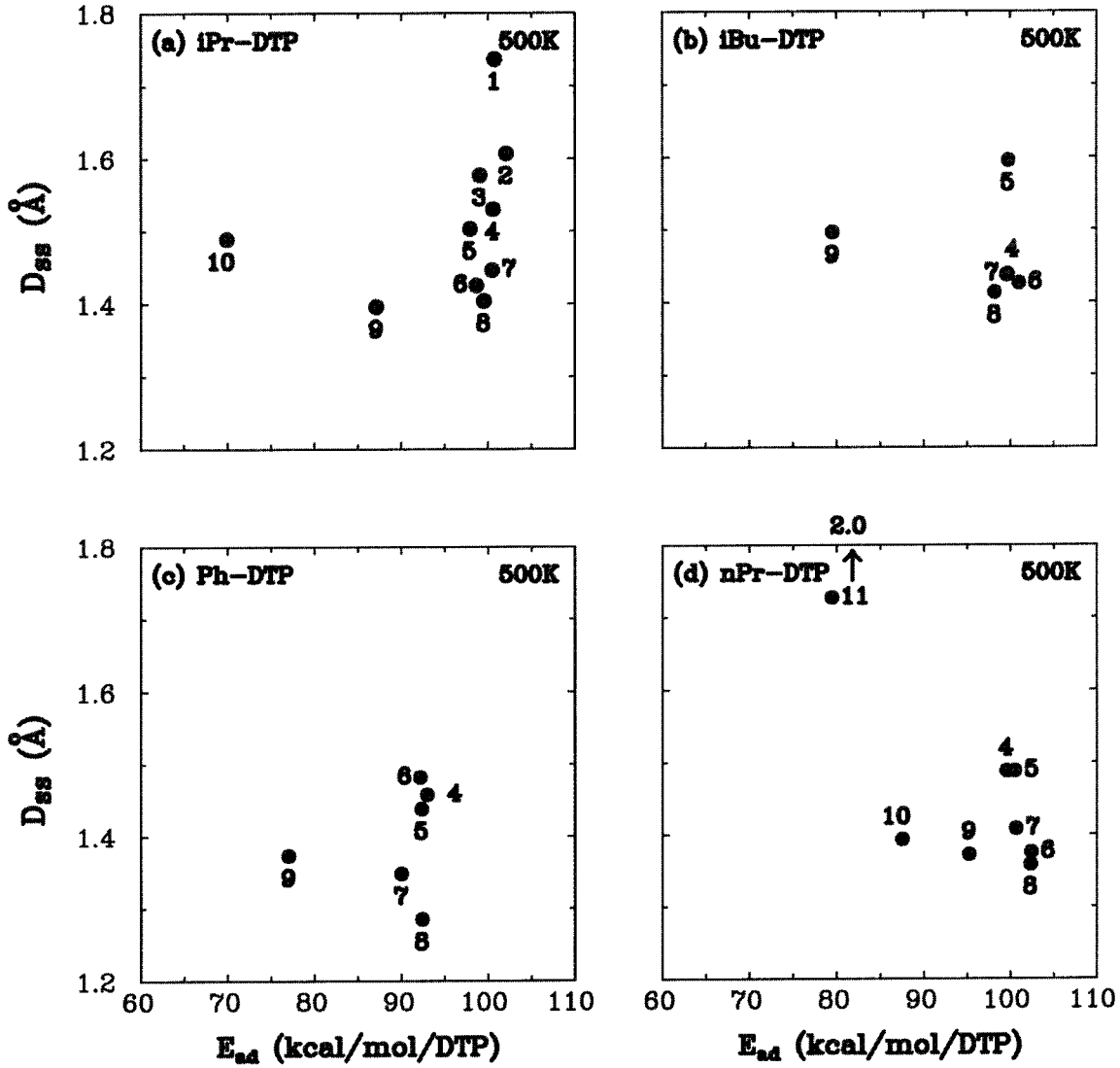

Figure 10. Sulfur-to-surface distance versus the adsorption energy for DTP molecules. The number of molecules adsorbed is indicated with each data point ($N = 8$ corresponds to $\theta = {}^1/_2$). We see that the D_{ss} decreases with coverage with nearly consistent adsorption energy up to $\theta = {}^1/_2$. With higher coverage the D_{ss} increases while the adsorbed energy drops dramatically.

diagonal of the parallelogram. The total energy of this structure is 120 kcal/mol higher than that of Figure 7b (15 kcal/mol DTP). However, starting with Figure 7c and rotating the S−Fe binding direction 60° leads to Figure 7d, which has all g^+ conformers but an energy similar to 7b (a total energy 32 kcal/mol lower). Therefore, case 7d with all g^+ conformers is as good as (perhaps slightly better than) case 7b with all g^- conformers. Both minimize the intramolecular interactions of the SAM.

Similarly, we can also achieve a good packing from a mixture of 50% g^+ and 50% g^- conformers by carefully alternating the S−Fe binding directions. Indeed, Figure 7e shows such a packing whose total energy is 2 kcal/mol lower than Figure 7b. Therefore, the packings in Figure 7b,d,e are energetically equivalent, although they are structurally different from one another.

III.C. Monolayer Thickness. The equilibrium shape of the adsorbed molecules changes considerably depending upon coverages. To characterize this transition, we examined the variation in monolayer thickness with coverage, which is estimated by the difference between the maximum and minimum coordinates of all atoms in each molecule in the direction perpendicular to the surface, averaged over time and over all molecules. The results for DTP are displayed in Figure 8, from which we can see that the monolayer thickness increases with the surface coverage above $\theta > {}^1/_4$.

Figure 9 shows side view of the SAM structures of *i*Pr from coverage $\theta = {}^1/_{16}-{}^5/_8$. At coverage $\theta < {}^1/_4$, some R groups are bent over to the surface and some upright. Adding a new molecule to the surface at these low coverages may cause more adsorbate molecules bent over to increase R group−surface interactions, which leads to a thinner monolayer. For higher coverages ($\theta > {}^1/_4$) stronger intramolecular interactions lead the R groups to a more upright orientation with respect to the surface, which results in an increase in the thickness. The longer the R group, the larger the increment of the thickness at high coverages.

III.D. Sulfur−Surface Distance. To determine how the bonding distance of the adsorbate molecules to the surface changes with the coverage, we calculated the average sulfur-to-surface distance D_{ss}. A plot of D_{ss} versus the adsorption energy of DTPs at various coverages is given in Figure 10, where each data point is averaged over the last 6 ps of MD simulation. For all four R groups, the decrease in D_{ss} with increased coverage for $\theta < {}^1/_2$ occurs. Then an increase in D_{ss} for $\theta > {}^1/_2$ that goes with the decreased bonding energy. The

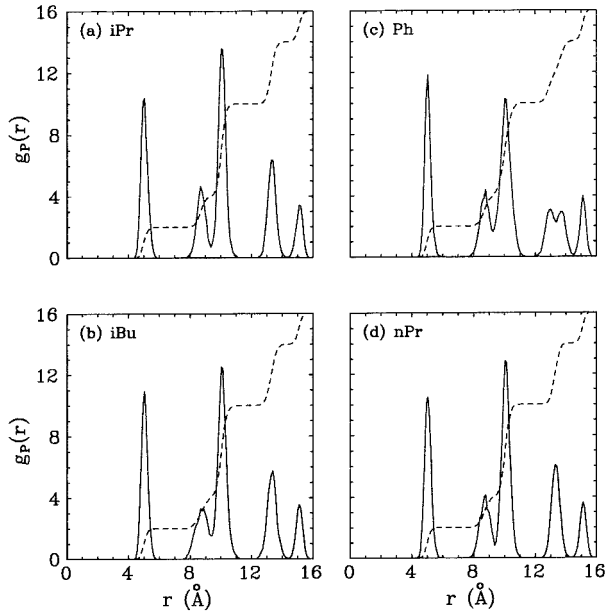

Figure 11. Two-dimensional radial distribution functions of DTP molecules at $^1/_2$ coverage (solid lines) and the corresponding integrated coordinate functions (dashed lines).

minimum D_{ss} coincides with the maximum bonding energy at $^1/_2$ coverage for these DTP molecules.

For *i*Pr the S−surface distance decreases monotonically from 1.73 to 1.4 Å as θ increases to $^1/_2$ but with relatively similar bonding energies. Then for $\theta = {}^9/_{16}$ the adsorption energies decrease by 10 kcal/mol but with no change in D_{ss}. However, by $\theta = {}^5/_8$ the adsorption energy has decreased by 30 kcal/mol and D_{ss} has increased by 0.1 Å.

From Figure 9 we see that at the coverages $\theta < {}^1/_2$ some *i*Pr groups bend over toward the surface, which may cause a slight increase in D_{ss} from its minimum value. As the coverage increases, more *i*Pr groups point straight up, which gives rise to tighter intramolecular interactions and reduces the sulfur to surface distance. However, after some critical coverage ($\geq$9 molecules), the surface are so densely packed that some molecules cannot get to the surface as close as the other molecules do. As a result, the value of D_{ss} increases significantly.

III.E. Two-Dimensional Radial Distribution Function. We also examined the two-dimensional radial distribution functions $g(r)$ of the DTP molecules at $^1/_2$ coverage. In these calculations we take the center of the DTP molecule as the P atoms. The resulting $g_P(r)$ for the four DTPs, averaged over 10 ps of MD, are shown in Figure 11. This figure also shows the integrated number of neighbors as a function of the radial distance. All four molecules exhibit a well ordered surface structure with (i) 2 first-nearest neighbors at 5 Å, (ii) 2 additional neighbors at 9 Å, and (iii) 6 additional neighbors at 10−11 Å. Since the adsorption is localized to the binding sites of the crystal surface, the structure in the distribution of the adsorbate molecules is crystal-like. The smoothness of $g_P(r)$ indicates the degree of order in the structures of these DTPs are essentially identical.

IV. Correlation of Results from Simulations with Wear Performance

Because of the great expense of engine experiments, it is important to obtain criteria for selecting the most promising materials prior to full engine tests. The SAM model[4] assumes that increased cohesive energy in the SAM is correlated with improved wear performance. Indeed this criteria is useful in suggesting new wear inhibitors.

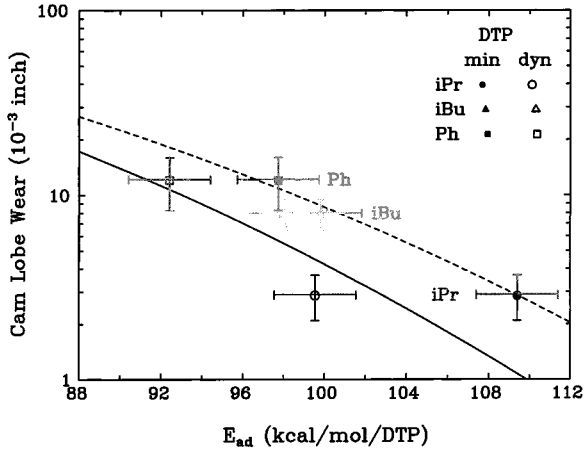

Figure 12. Correlation of SAM adsorption energy with cam lobe wear in Sequence IIID engine tests for commercial DTP molecules. The uncertainty in the adsorption energies is estimated as 2 kcal/mol/DTP. The solid/dashed curve is the least-squares fit of the MD/minimization results to the relation $w = a \exp(-bE_{ad}^3)$. Here, $a_{dyn} = 0.35$ in. and $b_{dyn} = 4.4 \times 10^{-6}$ (kcal/mol/DTP)$^{-3}$ for the dynamics fit, and $a_{min} = 0.30$ in. and $b_{min} = 3.6 \times 10^{-6}$ (kcal/mol/DTP)$^{-3}$ for the minimization fit.

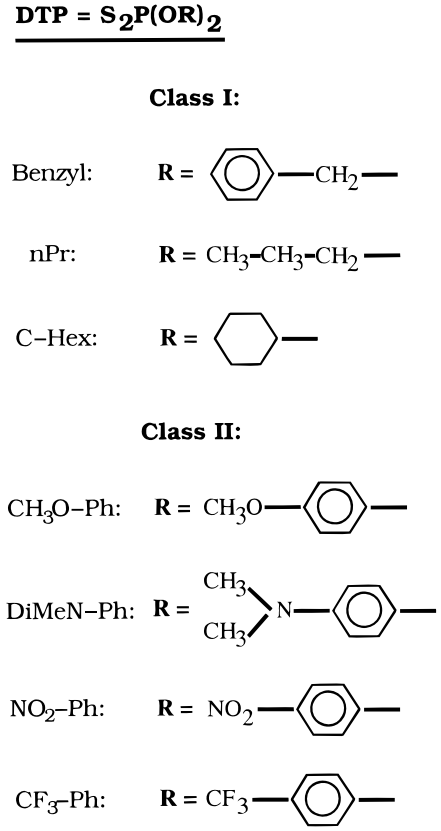

Figure 13. List of novel R groups for DTP tested with the SAM model.

IV.A. Commercial DTPs. Figure 12 compares the measured maximum cam lobe wear w in the sequence IIID tests[10b] against the adsorption energy E_{ad} at $\theta = {}^1/_2$ for the three commercial R groups of DTP. Results from both minimization and dynamics simulations are shown with the error bars, indicating the statistical errors in the experiment and the estimated errors of the calculation. We see that *i*Pr has the highest adsorption energy and the least wear (best antiwear performance), while Ph has the lowest adsorption energy and the greatest wear (poorest

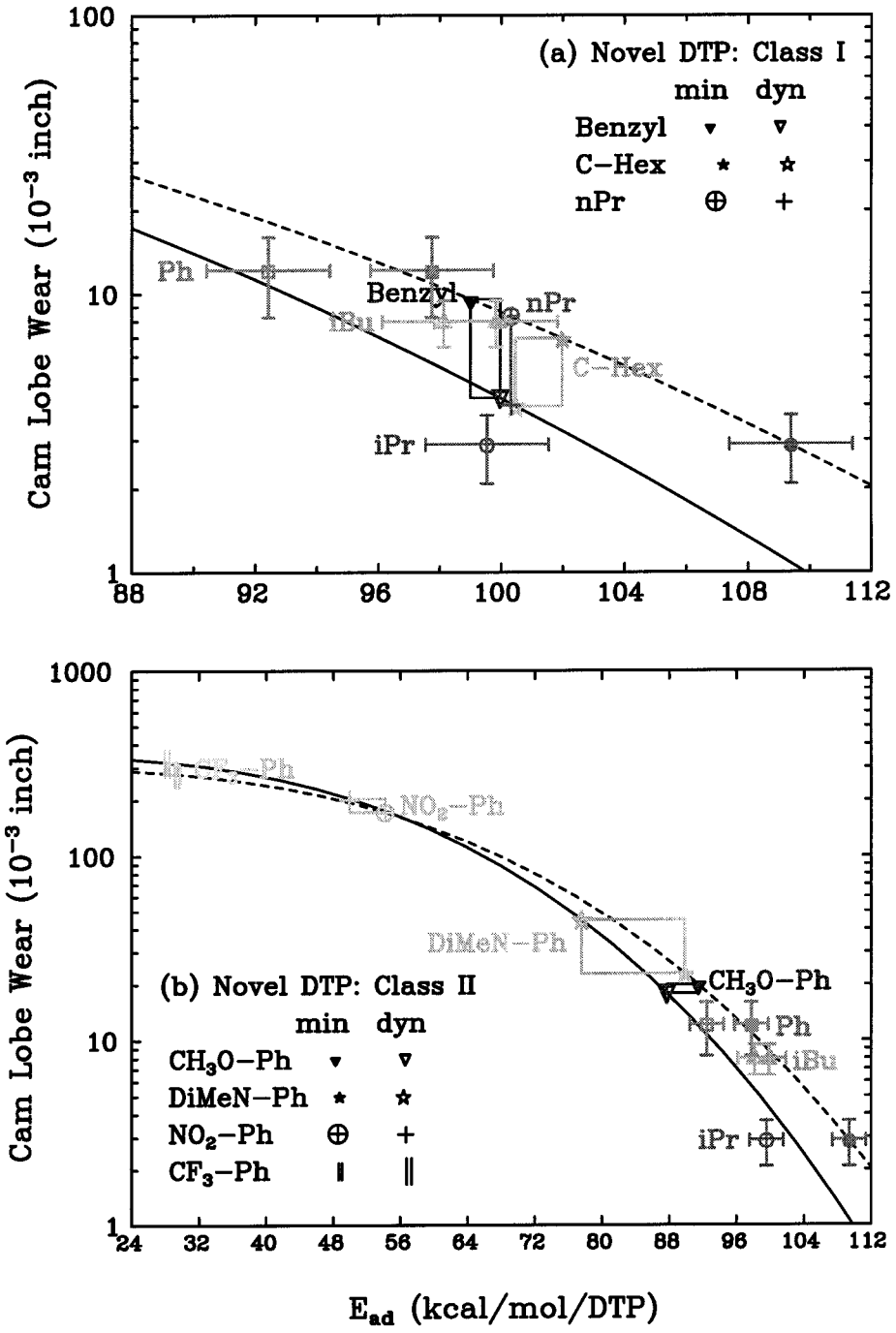

Figure 14. Adsorption energy versus wear for the novel DTP molecules listed in Figure 13: (a) class I (good wear) and (b) class II (bad wear). Boxes are drawn from the projection of the minimization and dynamics energy results on to the corresponding minimization and dynamics curves, respectively.

antiwear performance) while *i*Bu falls between for both measures. The MD results indicate that *i*Bu is closer to *i*Pr than to Ph, which is in a qualitative agreement with the engine test data where *i*Bu was found to provide low wear in the sequence IIID test (relatively high temperature) but high wear in the sequence VD test (relatively low temperature).[23b]

Over the range of E_{ad} for these inhibitors, the data can be fit with a linear relation $w = A - BE_{ad}$ with $A_{dyn} = 0.35$ in. and $B_{dyn} = -3.4$ (kcal/mol DTP)$^{-1}$ or $A_{min} = 0.09$ in. and $B_{min} = -0.8$ (kcal/mol DTP)$^{-1}$. However, for small E_{ad} comparable to the lubricant the wear should saturate whereas for very large E_{ad} it should go to zero. Hence, we used the following relation

$$w = a \exp(-bE_{ad}^{3}) \qquad (2)$$

for fitting the data. Hence, the wear approaches to zero as E_{ad} increases to infinity. The parameter a in (2) is the wear at $E_{ad} = 0$ (i.e., no inhibitor present). In fact, running the Sequence IIID test on an engine without any additives in the oil always leads to failure. From preliminary minimization calculations of E_{ad} for the pure oil case, we find the adsorption energy for a pure oil monolayer in the range from 6 to 15 kcal/mol. Taking the average value 12 kcal/mol as the E_{ad} of the pure oil and assuming that the wear at this condition is roughly 0.3 in. (which obviously would cause a failure in the engine test), and doing a least-squares fit to (2) leads to $a_{dyn} = 0.35$ in. and $b_{dyn} = 4.4 \times 10^{-6}$ (kcal/mol DTP)$^{-3}$ for the MD data set and $a_{min} = 0.30$ in. and $b_{min} = 3.6 \times 10^{-6}$ (kcal/mol DTP)$^{-3}$ for the minimization results.

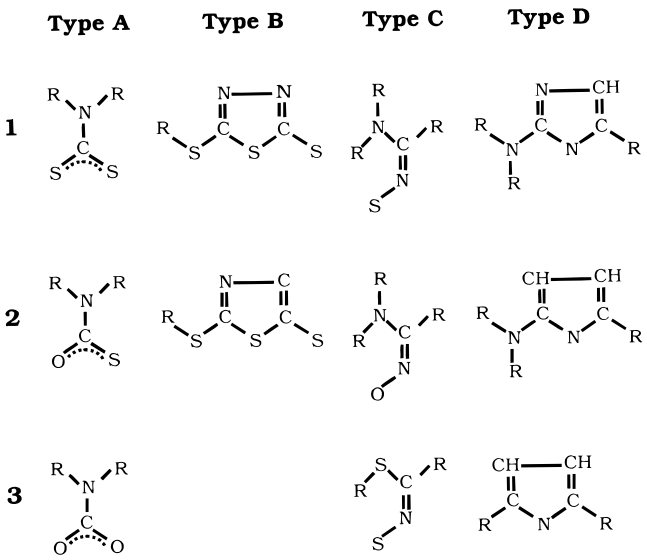

Figure 15. List of candidate wear inhibitors not containing phosphorus tested with the SAM model.

In the following we use the relations between the adsorption energy and wear derived here to predict (prior to engine tests) the antiwear performance of other interesting materials.

IV.B. Novel DTP. As an example on the application of the SAM model, we considered DTP molecules with novel R groups. The seven new R groups in Figure 13 were considered. On the basis of the SAM model, we classified these seven novel DTP molecules as class I (flexible linkage to O) and class II (phenyl attached to O). The predicted wear of these novel DTP molecules based on the SAM model are displayed in Figure 14. The boxes for each molecule are drawn from projecting the minimization and MD result of that molecule on to the minimization and dynamics curves, respectively. The MD simulations for these seven molecules are all 30 ps long.

As shown in Figure 14a, the adsorption energies of cyclo-hexyl, *n*Pr, and benzyl are in the same range defined by *i*Pr, *i*Bu, and Ph. The SAM model suggests that this class R groups should provide better performance than Ph. Particularly, the MD results of these molecules are close to or better than that of *i*Pr. Thus, they are expected to provide wear protection to surfaces as good as *i*Pr. Indeed, a single sequence IIID test for *n*Pr has been carried out,[23a] leading to an excellent antiwear performance (4.4×10^{-3} in. versus 2.9×10^{-3} in. for *i*Pr). This is very encouraging since the SAM model prediction is in excellent agreement with the engine test data for *n*Pr.

The class II DTP have much lower adsorption energies than Ph (Figure 14b). The SAM model suggests that the wear performances of these new molecules will be very poor. A common feature on all four class II molecules is that a phenyl group is attached directly to the oxygen. We believe that this leads to a much more rigid structure (as for Ph) so that the para-substituent of one molecule impacts the neighbors. In contrast, all three class I molecules have more flexible linkage to the oxygen. This includes cyclo-hexyl, *n*Pr, and benzyl.

V. Non-Phosphorus Containing Wear Inhibitors

To find molecules that do not contain P and yet have good wear performance, we extended the SAM model to the 11 chemical compounds in Figure 15. These calculations used methyl as the model R group and considered only the coverage at $\theta = {}^1/_2$. The results are summarized in Table 1, where we

TABLE 1: Relative Adsorption Energies (kcal/mol) of Types A−C Non-Phosphorus Molecules

	type A	type B[a]	type C	type D[b]
1	141	62	108	0
2	103	81	123	35
3	35		116	110

[a] Since Type B consists of three sulfur atoms and the FF parameters for S−Fe interaction are developed on the two sulfur (dithiophosphates) interaction, we carried out QM calculations to determine that the total energy of the SAM structure should be corrected by −88 kcal/mol. [b] For Type D, a correction of 22 kcal/mol has been added to the total energy to adjust to the QM results for N−Fe interactions.

see that A-1 (DTC), in which a C−N group is substituted for phosphorus in DTP, gives the largest cohesive energy. Thus, on the basis of the SAM model, DTC showed the best promise for a new wear inhibitor. Below, we will see that monolayers formed from the DTC molecules are energetically more favorably adsorbed on the iron-oxide surface than DTP, both with minimization (0 K) and dynamics (500 K). Indeed, both molybdenum DTP and molybdenum DTC are used in motor vehicles as friction modifiers.[12] After choosing DTC, we considered these six different R groups: (1) normal 3-, 5-, and 7-carbon chains (nC$_3$, nC$_5$, and nC$_7$) and (2) branched 3-, 5-, and 7-carbon chains (iC$_3$, iC$_5$, and iC$_7$) to investigate the relative performances of different carbon chains within the DTC class.

V.A. Adsorption Energy. We calculated the energetics at various concentrations for all the six groups. The results are shown in Figure 16. The cohesive and adsorption energy results for DTC molecules are somewhat different than the DTP results in Figure 5. For both the minimization and MD the adsorption energies of nC$_3$, iC$_3$, and iC$_5$ peak at $\theta = {}^1/_2$ and those of nC$_5$, iC$_7$, and nC$_7$ peak at $\theta = {}^3/_8$. In all the cases, the adsorption energy decreases significantly above $\theta = {}^1/_2$. This finding is basically consistent with the DTP results. That is, the optimal packing is approximately at $\theta = {}^1/_2$.

However, the total cohesive energies of the DTC molecules are maximum at different coverages for different R groups. Thus, the cohesive energy peaks at $\theta = {}^3/_4$ for nC$_3$ and nC$_5$, at $\theta = {}^{11}/_{16}$ for iC$_3$ and nC$_7$, and at $\theta = {}^9/_{16}$ for iC$_5$ and iC$_7$. Thus the optimal packing, if derived from the cohesive energy, would be at higher coverages than that inferred from the adsorption energy. In general, a greater number of linear chain molecules can be accommodated onto the surface than the corresponding branched chain molecules (in a agreement with the situation for *i*Pr vs *n*Pr DTP). For simplicity, we have used the adsorption energy as the criteria for choosing optimal packing. Consequently, we consider that the optimal coverages of these DTCs are all at ${}^1/_2$ coverage, just as for DTP.

For $\theta = {}^1/_2$ we find that the adsorption energies (at both minimization and 500 K), are in the sequence

$$i\text{C}_5 \approx n\text{C}_3 > i\text{C}_3 > n\text{C}_5 > i\text{C}_7 > n\text{C}_7$$

This ordering in adsorption energy among the six R groups of DTC may be understood from the size of the DTC molecules and the spacing of surface Fe sites in the iron-oxide lattice. The length in the tail elongation direction of a DTC molecule is ~6 Å for iC$_3$, 8 Å for nC$_3$, 10 Å for iC$_5$, 12 Å for nC$_5$, 14 Å for iC$_7$, and 15 Å for nC$_7$, respectively. Comparing them to the Fe−Fe spacing of ~5 Å, we found that iC$_5$ fits perfectly into the spacing of every two iron atoms. While iC$_3$ and nC$_3$ are a little bit shorter, the sizes of nC$_5$, iC$_7$, and nC$_7$ are much larger than the Fe−Fe spacing. Of course, the conformations of the carbon chains in the R groups may also play some role in

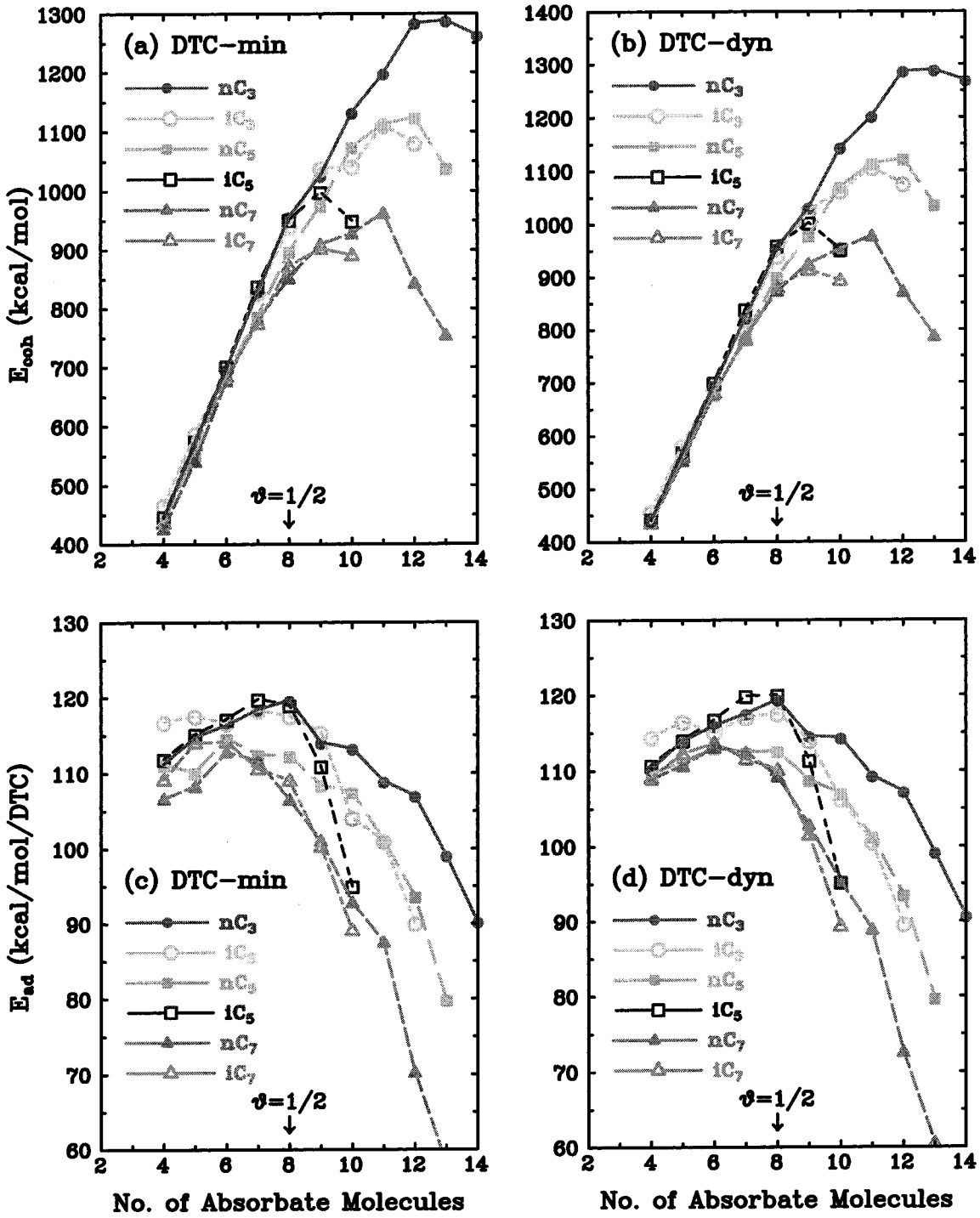

Figure 16. Cohesive enregy and adsorption energy as a function of surface coverage for DTC molecules: (a) E_{coh} from minimized structures, (b) E_{coh} from 10 ps of MD simulations at 500 K; (c) E_{ad} from minimized structures, and (d) E_{ad} from 10 ps of MD simulations at 500 K.

adjusting the lengths of the molecules. But for a system with strong chemical bonds to the surface such as in this case the spacing between the substrate binding sites is a dominant factor in priorizing what size of molecules forms an energetically favorable monolayer.

V.B. Packing Pattern. Figure 17 shows a top view of the minimized structures of iC$_5$ at various coverages. Comparing DTC with DTP, we see differences in the packing patterns. The packing of the DTP (Figure 4) is along the direction perpendicular to that defined by the two sulfur atoms of the molecules, whereas that of the DTC is in the same direction defined by the two sulfur atoms (Figure 17). This is due to the differences in the structures of these two types of molecules. As shown in Figure 18, substitution of the C−N in DTC for the P in DTP rotates the tail direction by 90°. Thus, DTP has tail chains extending perpendicular to the direction connecting the two S atoms, whereas in DTC they stretch parallel to the direction defined by the two S atoms. Of course, we can force the DTC tails in the same direction of the DTP tails. However, the energy would be increased by 21 kcal/mol if we did this by rotating C−N−C−C torsional angle and 3 kcal/mol by rotating the N−C−C−C torsional angle.

V.C. Monolayer Thickness. The variation of the monolayer thickness of these DTC molecules with coverage are displayed in Figure 19. We can see that the thickness increases consistently with the surface coverage and that the increments are larger for

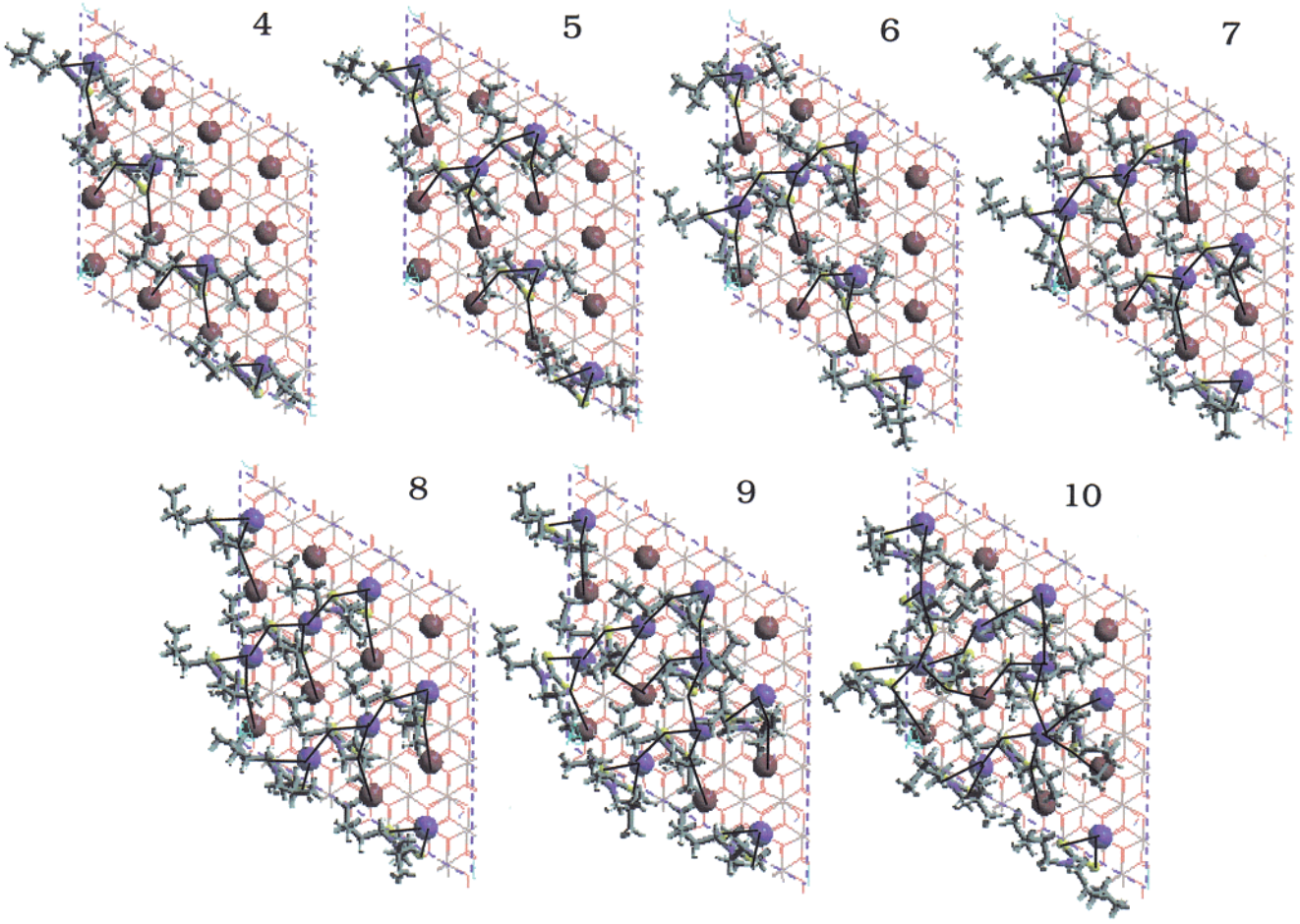

Figure 17. Top view of the SAM structure for 4 to 10 iC$_5$-DTC molecules on the surface (for symbols, see Figure 4).

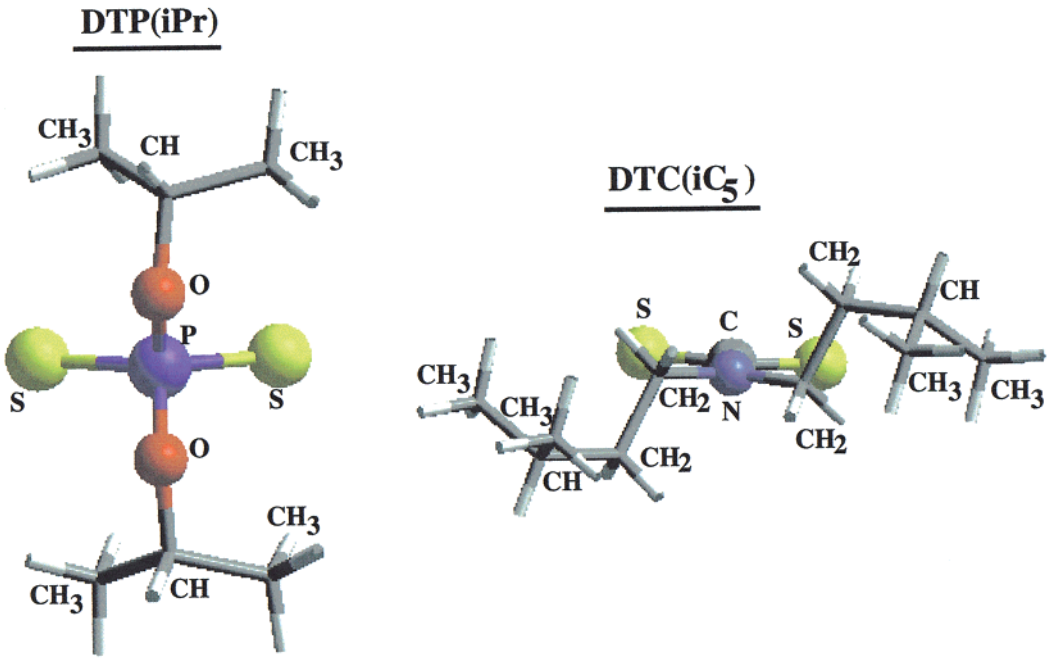

Figure 18. Structures of iPr-DTP and iC$_5$-DTC molecules in the gas phase. The head ligand atoms are shown as balls, and the hydrocarbon tail atoms as cylinders. The elongation of iPr molecule is normal to the direction connecting the two sulfur atoms, whereas that of iC$_5$ molecule is in the same direction defined by the sulfur atoms.

the longer carbon chains. It also appears that linear chains increase faster than branched chains do. The transition from the molecules bend over to the surface at low coverages to a more upright orientation at high coverages can be seen clearly in Figure 20, which shows the side view of the SAM structures of iC$_5$ between $\theta = {}^1/_4$ and ${}^5/_8$.

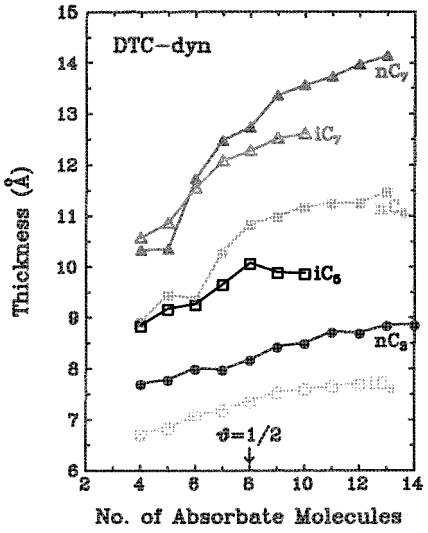

Figure 19. Monolayer thickness as a function of coverage for DTC molecules calculated from 10 ps MD at 500 K.

V.D. Sulfur−Surface Distance. Compared with Figure 10, the S-surface distance plot for DTCs in Figure 21 is a bit more complicated. For $\theta < {}^1/_2$, D_{ss} decreases monotonically with the coverage; however, the results for higher coverage depend on R. For iC$_7$ the D_{ss} begins to increase at $\theta = {}^1/_2$, whereas for iC$_5$ and iC$_3$ the smallest D_{ss} is at $\theta = {}^9/_{16}$. For nC$_3$, nC$_5$, and nC$_7$ the shortest D_{ss} is for $\theta = {}^{11}/_{16}$, but by this point the E_{ad} has decreased substantially ($\geq$10 kcal/mol) below that at $\theta = {}^1/_2$. It appears that even when the surface is highly packed, the adsorption energy has been significantly reduced, the DTC molecules can still be very close to the surface (i.e., the value of D_{ss} remains small). This effect is more pronounced for the normal chain molecules than for the branched chain molecules. Thus, although the surface-molecules interactions are still good at these high coverages, the ligand−ligand interactions are bad (due to steric effects) so that the net contribution to the adsorption energy is negative.

That DTP and DTC molecules respond differently to overpacking reflects the flexibility of the molecules. The surface can accommodate a higher concentration of more flexible molecules without penalizing D_{ss}, despite the overpacking that makes the energy unfavorable. Thus, DTC molecules are more flexible than DTP molecules and DTC molecules with normal carbon chains are more flexible than those with branched carbon chains.

V.E. Two-Dimensional Radial Distribution Functions. In calculating the two-dimensional $g(r)$ of the DTC molecules at

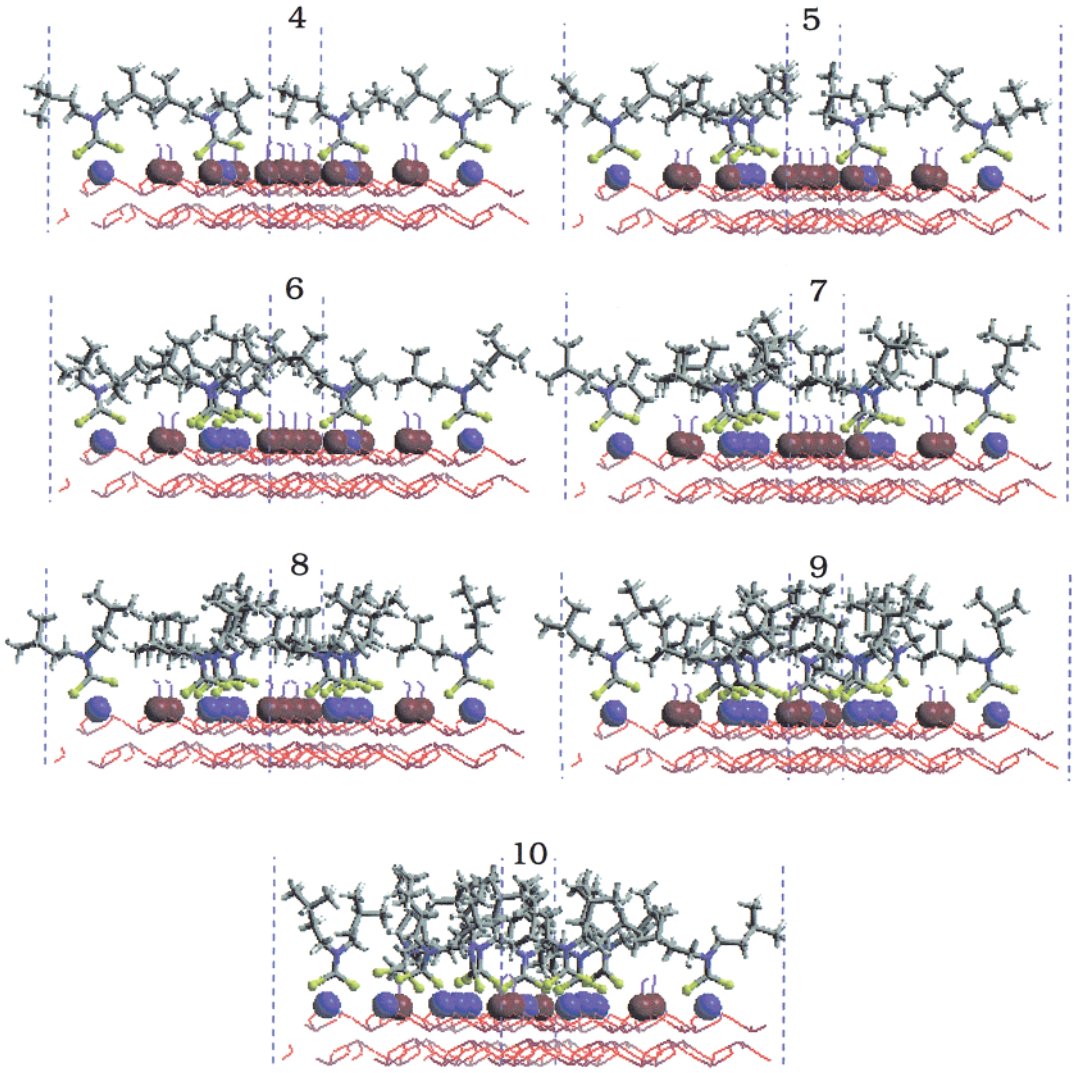

Figure 20. Side view of the SAM structure for four to ten iC$_5$-DTC molecules on the surface (symbols same as in Figure 4).

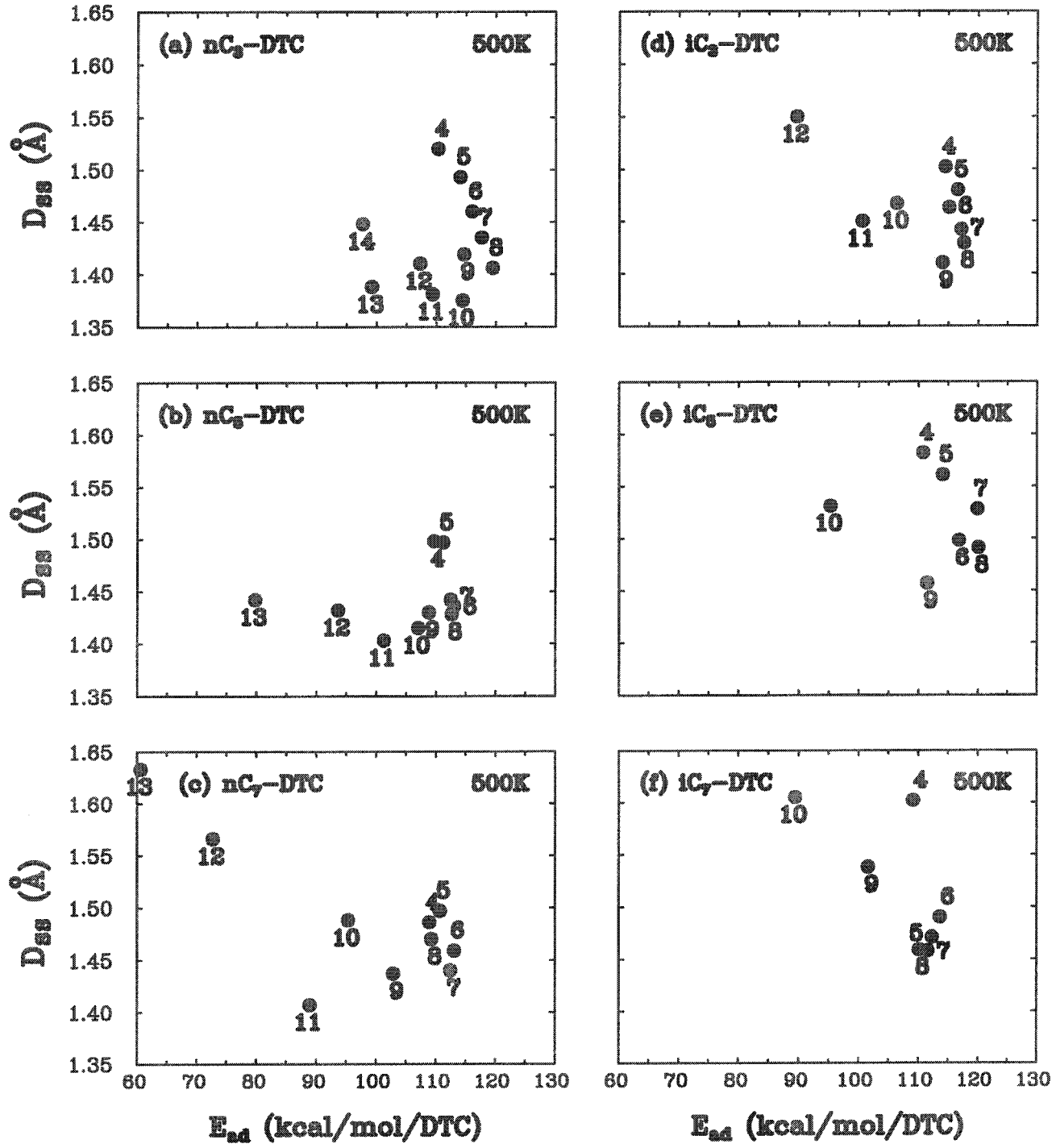

Figure 21. Sulfur-to-surface distance versus the adsorption energy for DTC molecules. The number of molecules adsorbed is indicated with each data point ($N = 8$ corresponds to $\theta = {}^1/_2$).

$^1/_2$ coverage we took the center of the molecule as the C−N bond midpoint. The resulting $g_{C-N}(r)$ are shown in Figure 22. We can see that, in contrast to DTP, these DTC molecules show considerable differences in the degree of order in their structures. The broader and smaller peaks for nC$_7$ and iC$_7$ indicate that these molecules jiggle extensively during the dynamics. Thus, the monolayer structures of nC$_7$ and iC$_7$ are the least ordered, while iC$_5$ and nC$_3$ are the most ordered. The monolayers of iC$_3$ and nC$_5$ have an intermediate behavior. Interestingly, this ordering in the structure of $g_{C-N}(r)$ correlates remarkably well with the relative adsorption energies of the DTC molecules discussed earlier.

V.F. Predicted Wear Performance. The calculated adsorption energies for these six R groups of DTC are given in Figure 23. The adsorption energies of all the DTC molecules are 10−20% larger than those for the DTP molecules. Using the correlation curves between adsorption energy and wear obtained from the DTP suggests that the DTC molecules should lead to less wear than the DTP molecules. Within the DTC class, we see that iC$_5$ and nC$_3$ have the largest adsorption energy (lowest wear) followed by iC$_3$. However, the adsorption energies of nC$_5$, iC$_7$, and nC$_7$ are much lower, suggesting poorer performance. The results from the minimization at 0 K and MD simulations at 500 K give a consistent ordering for these molecules. Thus,

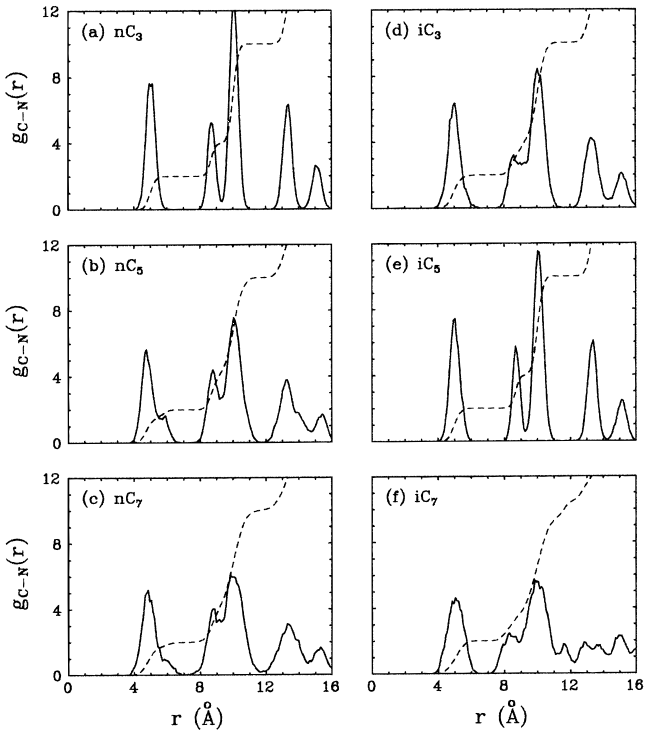

Figure 22. Two-dimensional radial distribution functions of DTC molecules at $^1/_2$ coverage (solid lines) and the corresponding integrated coordinate functions (dashed lines).

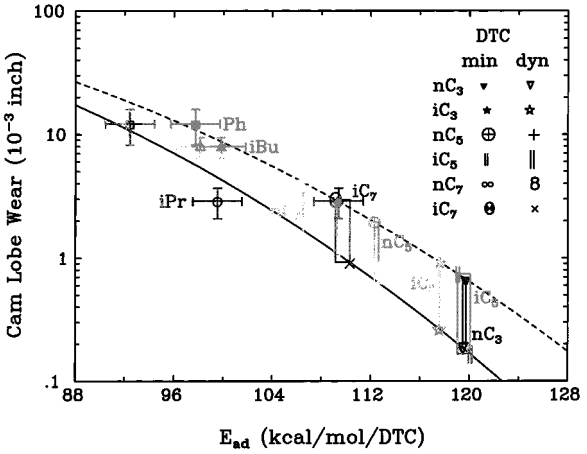

Figure 23. Adsorption energy versus wear for DTC molecules: three normal chains, nC$_3$, nC$_5$, and nC$_7$, and three branched chains, iC$_3$, iC$_5$, and iC$_7$.

we expect that iC$_5$, nC$_3$, and iC$_3$ should provide better wear inhibitor than nC$_5$, iC$_7$, and nC$_7$. The SAM model seems to indicate that molecules with short chain lengths (<10 Å) are better than that of longer chains. This result is consistent with the conclusion of a study by Born et al.[11] They investigated DTP molecules with a wide variety of R groups and found that the effectivenesses of the DTP molecules for beyond six carbons R groups are poorer than those containing less than six carbon chains.

VI. Conclusions

The wear protection of engine surfaces provided by zinc dithiophosphates involves a number of complex issues involving film formation and stability at a variety of temperatures and pressures. It may be affected by shear strain and transient behavior. We have isolated just one of the factors—the stability of the SAM at 500 K—which seems to correlate with observed wear performance. On the basis of this criterion we have suggested new experiments.

Using the force field developed from first-principles calculations, we find that the DTP and DTC molecules form a monolayer at $\sim^1/_2$ coverage with a nearly constant adsorption energy up to this point which then decreases rapidly at higher coverages. Furthermore, the adsorption energies at $^1/_2$ coverage for various DTP molecules correlate (inversely) with the wear data measured in engine tests.

We considered other novel R groups and concluded that the α carbon (attached to the O) should be flexible to have good wear performance. In particular, we find that R = c-hexyl and *n*-Pr, and benzyl are good candidates.

We identified DTC molecules as a possible nonphosphorus containing substitutes for DTP. They lead to relatively large adsorption energies on the iron-oxide surface. Among the six different R groups of DTC investigated, iC$_5$ and nC$_3$ have the largest adsorption energy, followed by iC$_3$. The other three R groups, nC$_5$, iC$_7$, and nC$_7$, have relatively smaller adsorption energies. Hence, iC$_5$ group, as well as nC$_3$ and iC$_3$, is likely the good candidate material for wear inhibitors.

Acknowledgment. This research was supported by the Chevron Chemical Company (Oronite Technology group). It was also supported by grants from the DOE-BCTR and NSF (CHE 95-12279). The facilities of the MSC are also supported by grants from DOE-ASCI, BP Chemical, ARO-MURI (Kiserow), Beckman Institute, Seiko-Epson, Exxon, Avery-Dennison Corp., NASA/Ames, Chevron Petroleum Technology Co., Asahi Chemical, NASA/JPL, Owens-Corning, and Chevron Research Technology Co. We thank Larry Smarr for access to the NCSA system for some calculations.

References and Notes

(1) Freuler, H. C., U.S. Patent 2364283, 1944.

(2) Jiang, S.; Dasgupta, S.; Blanco, M.; Frazier, R.; Yamaguchi, E. S.; Tang, Y.; Goddard, W. A., III *J. Phys. Chem.* **1996**, *100*, 15760.

(3) Liston, T. V. *Lubr. Eng.* **1992**, *May*, 389.

(4) Jiang, S.; Frazier, R.; Yamaguchi, E. S.; Blanco, M.; Dasgupta, S.; Zhou, Y.; Çağın, T.; Tang, Y.; Goddard, W. A., III *J. Phys. Chem. B* **1997**, *101*, 7702.

(5) Dacre, B.; Bovington, C. B. *ASLE Trans.* **1983**, *25*, 546. *ASLE Trans.* **1983**, *26*, 33.

(6) Fuller, M.; Yin, Z.; Kasrai, M.; Bancroft, G. M.; Yamaguchi, E. S.; Ryason, P. R.; Willermet P. A.; Tan, K. R. *Tribol. Int.* **1997**, *30*, 305.

(7) Yamaguchi, E. S.; Ryason, P. R. *Tribol. J.* **1996**, *3*, 123.

(8) Rappé, A. K.; Casewit, C. J.; Colwell, K. S.; Goddard, W. A., III.; Skiff, W. M. *J. Am. Chem. Soc.* **1992**, *114*, 10024.

(9) Plaza, S. *ASLE Trans.* **1987**, *30*, 233.

(10) (a) Roby, S. H. *Lubr. Eng.* **1991**, *47*, 413. Benchaita, M. T. *Lubr. Eng.* **1991**, *47*, 893. (b) McGeehan, J. A.; Yamaguchi, E. S.; Adams, J. Q. *SAE, Warrendale, PA* **1985**, *SAE 852133*. McGeehan, J. A.; Yamaguchi, E. S. *SAE, Warrendale, PA* **1989**, *SAE 892112*. McGeehan, J. A.; Graham, J. P.; Yamaguchi, E. S. *SAE, Warrendale, PA* **1990**, *SAE 902162*.

(11) Born, M.; Hipeaux, J. C.; Marchand, O.; Parc, G. *Lubr. Sci.* **1992**, *4*, 93.

(12) Yamamoto, Y.; Gondo, S. *Tribol. Trans.* **1989**, *32*, 251. Gondo, S.; Yamamoto, Y. *Jpn. J. Tribol.* **1991**, *36*, 323. Yamamoto, Y.; Gondo, S. *Tribol. Trans.* **1994**, *37*, 182.

(13) Ramachandran, S.; Tsai, B. L.; Blanco, M.; Chen, H.; Tang, Y.; Goddard, W. A., III *Langmuir* **1996**, *12*, 6419.

(14) Ramachandran, S.; Tsai, B. L.; Blanco, M.; Chen, H. J.; Tang, Y.; Goddard, W. A., III In *New Techniques for Characterizing Corrosion and*

Stress Corrosion; Jones, R. H., Baer, D. C., Eds.; The Minerals, Metals & Materials Society: Warrendale, PA, 1996; p 117.
(15) Mayo, S. L.; Olafson, B. D.; Goddard, W. A., III *J. Phys. Chem.* **1990**, *94*, 8897.
(16) Rappé, A. K.; Goddard, W. A., III *J. Phys. Chem.* **1991**, *95*, 3358.
(17) Wyckoff, R. W. G. *Crystal Structures*; Interscience: New York, 1963.
(18) Eggleston, C. M.; Hochella, M. F., Jr. *Am. Mineral.* **1992**, *77*, 911.
(19) *Cerius*^{2}, Molecular Simulations, Inc.: San Diego, California, 1997.
(20) Karasawa, N.; Goddard, W. A., III *J. Phys. Chem.* **1989**, *93*, 7320. Chen, Z. M.; Cagin, T.; Goddard, W. A., III *J. Comput. Chem.* **1997**, *18*, 1365.
(21) Nosé, S. *Mol. Phys.* **1984**, *52*, 255. Nosé, S. *J. Chem. Phys.* **1984**, *81*, 511. Hoover, W. G. *Phys. Rev. A*, **1985**, *31*, 1695.
(22) Ertl, G. In *The Nature of the Surface Chemical Bond*; Rhodin, T. N., Ertl, G., Eds.; North-Holland: Amsterdam, 1990.
(23) (a) Yamaguchi, E. S. *Internal Report*; Chevron Research Co.: Richmond, CA, 1981. (b) Yamaguchi, E. S., Private communication.